

Observation of Thermal Deuteron-Deuteron Fusion in Ion Tracks

K. Czerski¹, R. Dubey¹, A. Kowalska², G. Haridas Das¹, M. Kaczmarski¹, N. Targosz-Sleczka¹,
M. Valat¹

¹ Institute of Physics, University of Szczecin, 70-453 Szczecin, Poland

² Physics Department, Maritime University of Szczecin, 70-500 Szczecin, Poland

Abstract:

A direct observation of the deuteron-deuteron (DD) fusion reaction at thermal meV energies, although theoretically possible, is not succeeded up to now. The electron screening effect that reduces the repulsive Coulomb barrier between reacting nuclei in metallic environments by several hundreds of eV and is additionally increased by crystal lattice defects in the hosting material, leads to strongly enhanced cross sections which means that this effect might be studied in laboratories. Here we present results of the $^2\text{H}(\text{d},\text{p})^3\text{H}$ reaction measurements performed on a ZrD_2 target down to the lowest deuteron energy in the center mass system of 625 eV, using an ultra-high vacuum accelerator system, recently upgraded to achieve high beam currents at very low energies. The experimental thick target yield, decreasing over seven orders of magnitude for lowering beam energies, could be well described by the electron screening energy of 340 eV, which is much higher than the value of about 100 eV for a defect free material. At the energies below 2.5 keV, a constant plateau yield value could be observed. As indicated by significantly increased energies of emitted protons, this effect can be associated with the thermal DD fusion. A theoretical model explains the experimental observations by creation of ion tracks induced in the target by projectiles, and a high phonon density which locally increases temperature above the melting point. The nuclear reaction rate taking into account recently observed DD threshold resonance agrees very well with the experimental data.

1. Introduction

Nuclear reactions between charged particles at very low energies are determined by the penetration probability through the Coulomb barrier, which leads to dropping reaction cross section for lowering projectile energies. Its height can be, however, significantly reduced due to the inevitable presence of surrounding electrons. This so-called electron screening effect can be observed for single atoms, molecules and condensed-matter conditions and results in an exponential like enhancement of reaction cross sections at decreasing energies when compared to the bare nuclei case [1]. A particularly strong effect could be observed for metallic environments in both direct [2,3,4] and inverse reaction kinematics [5], where quasi-

free conduction electrons make the largest contribution. Therefore, these experiments are also of great importance for testing the electron screening effect in astrophysical plasmas, where the nuclear rates can be enhanced by many orders of magnitude [6]. In this context, deuteron-deuteron (DD) fusion reactions are of particular interest due to their relatively low Coulomb barrier of around 350 keV and their potential use as a future fusion energy source. The electron screening energy in these reactions, corresponding to the reduction of the Coulomb barrier, is larger than 100 eV for heavier metals and can be further increased three- or four-fold by crystal lattice defects [7,8].

On the other hand, recent accelerator studies on the DD fusion at very low energies strongly supports existence of a threshold resonance in ${}^4\text{He}$ placed at the excitation energy of about 23.8 MeV [7,9], which is responsible for a further enhancement of the reaction cross sections. Based on the first observation in the ${}^2\text{H}(\text{d},\text{p}){}^3\text{H}$ reaction of interference effects between the narrow single particle 0^+ resonance and known broad resonances, a large partial width of this resonance for the internal e^+e^- pair production has been predicted [9]. A corresponding observation of emitted electron/positron energy spectra using a single Si detector could be presented in full agreement with theoretical predictions [10,11]. New experiments performed with large volume NaI scintillation detector and HPGe detector also confirm emission of high energy bremsstrahlung as well as the associated excess of the positron annihilation line [12]. A direct consequence of recent studies is that the fusion of two deuterons can take place with probabilities that enables its observation at thermal meV energies.

In this letter, we present new experimental results of the ${}^2\text{H}(\text{d},\text{p}){}^3\text{H}$ reaction measured for the first time at the lowest deuteron beam energy of 1.25 keV (0.625 keV in CMS) applying a deuterated ZrD_2 target and the recently upgraded accelerator system with ultra-high vacuum at the University of Szczecin, Poland. For some other metallic targets, this reaction was previously studied at deuteron energies down to 3 keV and for PdO to 2.5 keV [13]. The electron screening results in an exponential-like enhancement of reaction cross sections for lowering projectile energies due to change of the penetration factor which can be estimated for the s-wave partial wave as follows:

$$P_{scr}(E + U_e) = \sqrt{\frac{E_G}{E + U_e}} \exp\left(-\sqrt{\frac{E_G}{E + U_e}}\right), \quad (1)$$

where the screening energy U_e has been added to the center mass energy E of reacting nuclei. The Gamow energy $E_G = 2(Z_1 Z_2 \pi / 137)^2 \mu$ is equal to 986 keV for the DD system (μ stays for the reduced mass). The reaction cross section can be then obtained using the expression for the penetration factor and the astrophysical S-factor $S(E)$:

$$\sigma_{scr}(E) = \frac{1}{\sqrt{E(E + U_e)}} S(E) \exp\left(-\sqrt{\frac{E_G}{E + U_e}}\right) = \frac{1}{\sqrt{E_G E}} S(E) P_{scr}(E + U_e) \quad (2)$$

The screening energy determined for the ${}^2\text{H}(\text{d},\text{p}){}^3\text{H}$ reaction on deuterated Zr target varies between 100 and 400 eV depending on the crystal lattice vacancies of the hosting material [7,8]. Whereas the lower value has been achieved for targets which were cleaned and amorphized by argon sputtering immediately before the measurements and agrees very well with theoretical predictions [14], the higher screening energy has been observed during long term experiments, producing a large number of crystal vacancies. This kind of the host material structure leads to localization of conduction electrons and an increase of the effective electron mass resulting in an increase of the screening energy [15].

According to the formulas above, the cross section of the ${}^2\text{H}(\text{d},\text{p}){}^3\text{H}$ reaction at $E=1$ keV should be enhanced compared to the bare nuclear case ($U_e = 0$) by a factor 4 or 300 depending on the screening energy equal to 100 or 400 eV, respectively. In both cases, determination of the screening energy would be much more exact if the measurements could be performed at the lowest possible energies. In the previous experiment [7], $E=3$ keV could be reached, and the enhancement factor of about 2 could be observed.

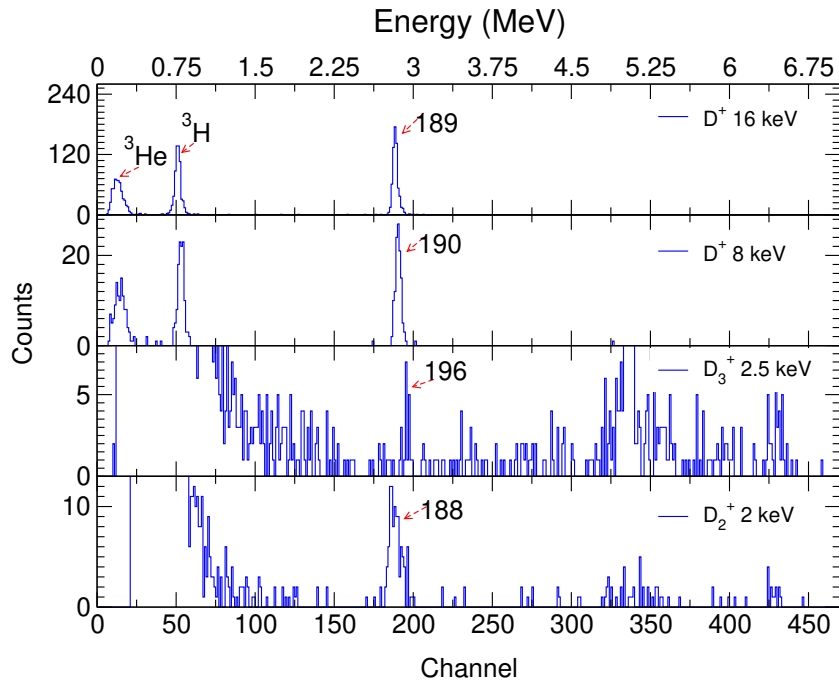


Fig. 1: Charged particle spectra of the ${}^2\text{H}(\text{d},\text{p}){}^3\text{H}$ reaction at different deuteron energies, applying atomic and molecular deuterium beams. The numbers at the proton line show the channel number of the peak position (for comparison see Fig. 2b). One channel corresponds to about 15 keV.

2. Results

2.1 Low-energy thick target yield

Measurements at the lowest deuteron energies were possible due to use of a new deceleration lens system allowing to operate the ECR ion source at relatively high voltages

with high beam currents. Atomic, D_2^+ and D_3^+ molecular ion beams have been applied to determine the thick target yield in a broad energy range of deuterons between 1.25 keV and 25 keV (0.625 keV and 12.5 keV in CMS). A low noise PIPS Si detector placed backwards to the beam at 135° was used to detect the emitted charged particles. For details see the Methods section. The experimental spectra and final results are presented in Fig.1 and 2. The experimentally measured thick target yield, defined as a sum of contributions resulting from different target depths up to the projectile range R , can be calculated with the formula:

$$Y_{scr}(E) = N_0 \int_0^R \sigma_{scr}(E) dx = N_0 \int_0^E \frac{\sigma_{scr}(E)}{|dE/dx|} dE \simeq \frac{2N_0 S(E)}{C\sqrt{E_G}} \exp\left(-\sqrt{\frac{E_G}{E+U_e}}\right) \quad (3)$$

where the stopping power function in the energy region studied is governed by the electronic stopping $|dE/dx| = C\sqrt{E}$ and N_0 stays for the deuteron number density in the target.

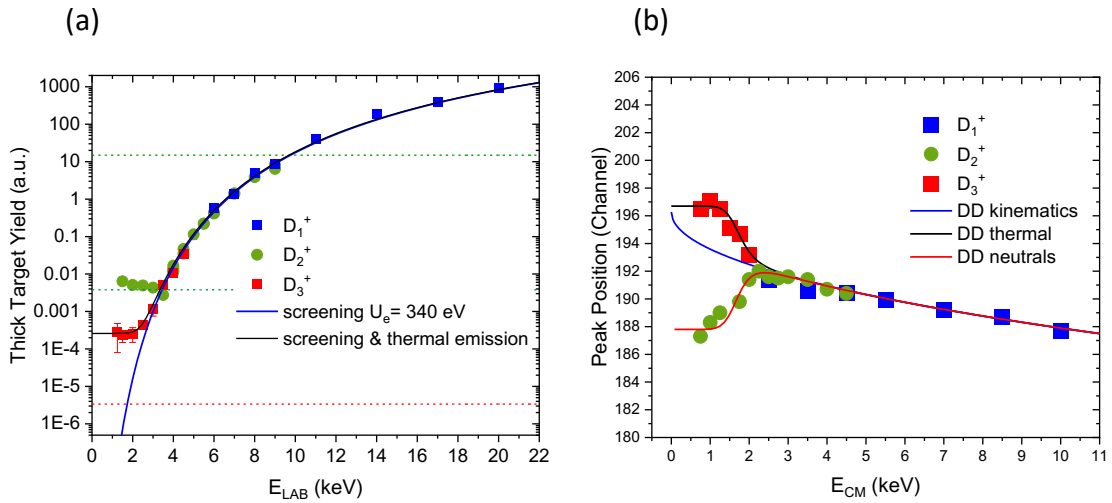


Fig. 2: (a) Thick target yield of the $^2\text{H}(\text{d},\text{p})^3\text{H}$ reaction. The blue full line corresponds to the theoretical screening curve (Eq. 3) obtained for the screening energy $U_e=340\pm30$ eV. The upper horizontal green dashed line shows the yield value measured with D_2^+ beam at $E_{LAB}=10$ keV per deuteron without using deceleration system. The lower green dashed line represents the yield value measured in the plateau region using the deceleration system, resulting from the neutralized beam fraction. The ratio of both yield values determines the neutralization factor of the beam, which is about 3×10^{-4} . The red dashed line corresponds to the expected yield for the neutralized D_3^+ beam compared to the value obtained at $E_{LAB}=4$ keV per deuteron without deceleration. However, the observed yield plateau is almost two orders of magnitude higher. The error bars of experimental points represent statistical uncertainty only. The systematic uncertainty due to deuteron density in the target is of about 10%. (b) Channel number of the proton peak position. At the lowest deuteron energies, the experimental data obtained with the D_3^+ beam can be described by thermal emission ($E=0$) and the fast-decreasing component corresponding to the screening curve from Fig. 2a (black curve). The neutral yield component for the D_2^+ beam can be described similarly by the red curve. High energy points follow the energies resulting from the kinematics of the $^2\text{H}(\text{d},\text{p})^3\text{H}$ reaction (blue curve, see the Methods section).

The experimental thick target yield decreases over the measured energy range by 7 orders magnitude following a theoretical screening curve (Eq. 3) assuming a constant

astrophysical S-factor of 57 keV barn [16] and the fitted screening energy of 340 ± 30 eV. The smallest yield value could be measured using the D_3^+ beam at the deuteron energies 2.0 keV corresponding to the cross section of about 100 ± 20 pbarn. For lower deuteron energies, a constant plateau in the thick target yield was observed. Similar plateaus could also be detected at higher deuteron energies for D_1^+ and D_2^+ beams, clearly coming from a small number of ions neutralized at a distance of 1.5 m between electric steerers and the deceleration lenses and the target on the residual deuterium gas (see Fig. 6 in Methods section). The neutral atom contribution to both beams could be determined to be of about 3×10^{-4} by comparison of the reaction yields measured with and without deceleration at the same ion source potential (see the green horizontal dashed lines in Fig. 2a and 7a). This number agrees with a theoretical estimation assuming the known neutralization cross section [17,18] of 10^{-15} cm 2 for all deuteron beam species on the D_2 rest gas and the vacuum pressure of about 8×10^{-9} mbar in this part of beam line. Thus, a corresponding thick target yield induced by neutral deuteron atoms during the D_3^+ beam irradiation would be expected about two orders of magnitude below the observed plateau level (red horizontal dashed line in Fig. 2a), underlying its different origin.

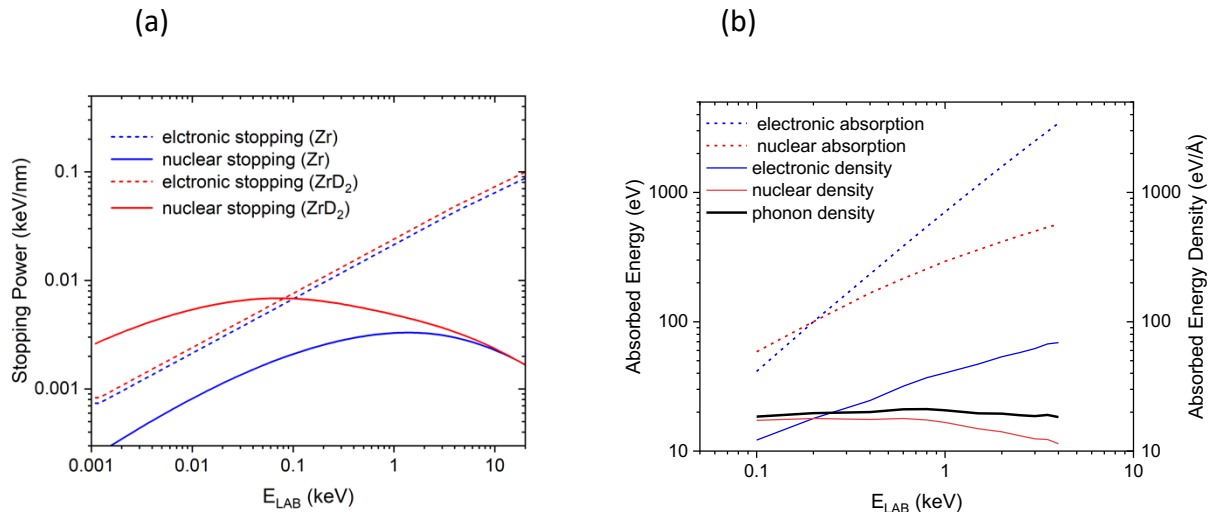


Fig. 3: (a) Nuclear and electronic stopping powers obtained for deuterons on Zr and ZrD_2 targets. (b) Deuteron beam energy absorbed by the ZrD_2 target due to nuclear and electronic stopping power (upper dashed curves). Electronic (full blue line) and nuclear (full red line) energy densities calculated as the corresponding absorbed energy divided by the range of the deuteron beam. The black line represents the total phonon density resulting from a sum of the nuclear energy density and 10% electronic energy densities, due to the electron-phonon coupling. The phonon density is almost constant at low deuteron energies. Calculations have been performed using the SRIM/TRIM code [19].

The energy dependence of the position of the 3 MeV proton peak on the energy of the deuteron beam may provide a conclusive argument about the mechanism of the ${}^2H(d,p){}^3H$ reaction. Since the Si detector was placed backwards from the beam, the proton peak should shift towards higher energies for lower deuteron energies according to the reaction

kinematics, considering the center mass system moves forwards (blue curve in Fig. 2b, see also the Methods section). However, for the D_2^+ beam, we observe a completely different result – in the region of plateau, the proton peak energy moves to lower energies indicating higher deuteron beam energies. The observed proton peak energies correspond to values expected for neutral atoms which were not decelerated by the electric lens system in the front of the target chamber. The red curve in Fig. 2b, takes into account the constant neutral atom fraction in the D_2^+ beam and the ionic component which is responsible for the strongly decreasing thick target yield with the screening energy of 340 eV (blue curve in Fig. 2a). In the case of irradiation with the D_3^+ beam, the proton peak position systematically takes much larger energy values, which excludes a significant contribution of neutral atoms. The corresponding proton peak energies are higher than the kinematics curve predicts. They can be calculated as a weighted average from the peak position resulting from the reaction kinematics (related to the strongly decreasing screening yield curve for $U_e=340$ eV) and the constant value representing the plateau yield contribution of protons emitted from the resting center mass system ($E_{CM}=0$) (see the Methods section). This finding suggests that the protons are emitted from the $^2H(d,p)^3H$ reaction occurring at thermal energies.

2.2 Thermal nuclear reaction rate

The theoretical cross section at thermal energies (lower than the screening energy) is governed by the 0^+ threshold resonance. The resonance energy is not exactly known and should be in the range [9] of 1 eV. New measurements of the internal e^+e^- pair creation (IPC) in the DD reaction give an estimation for the total resonance width of 700 meV – with a branching ratio between IPC and the proton partial widths [12] of about 14. In this energy region, the penetration factor is constant (see Eq. 3) and therefore, one can expect a plateau in the thick target yield for thermal energies. However, it should only take place at deuteron energies lower than the screening energy with the reaction yield 8 orders of magnitude lower than that observed in the present experiment [8]. The experimental data suggest that plateau protons are emitted from the DD center mass system moving with energy close to zero. Thus, it is convincing to assume that the bombarding deuterons produce a collision cascade and locally heat the deuterated Zr target to higher temperatures, which would enable a large number of deuterons to move within the crystal lattice and collide there with other deuterons. This mechanism would strongly increase the active volume of the target compared to the standard dynamics of the ion beam, for which only deuterons with the highest energies at the most top target layers contribute. Whereas the latter can be described by thick target yield proportional to the atomic number density, the former uses the nuclear reaction rates being characteristic for plasma physics with a quadratic dependence on N :

$$\mathcal{R}(T) = \frac{N^2}{2} \langle \sigma v \rangle = \frac{N^2}{2} \frac{(8/\pi)^{1/2}}{\mu^{1/2}(kT)^{3/2}} \int_0^\infty \sigma(E) E \exp(-E/kT) dE =$$

$$= N^2 \frac{16\pi^{3/2} \hbar^3 E_R^{1/2}}{\mu^2 a (kT)^{3/2}} (E_G/U_e)^{1/2} \exp[-(E_G/U_e)^{1/2}] \exp(-E_R/kT) \frac{\Gamma_p}{\Gamma} \quad (4)$$

where the Maxwell-Boltzmann velocity distribution and the Breit-Wigner formula for the single-particle threshold resonance have been applied (see the Methods section). Γ_p and Γ stay for the partial proton and total resonance widths, respectively. E_R is the threshold resonance energy (see the Methods section).

The nuclear reaction rate at thermal energies (Eq. 4) is the standard formula used in the nuclear astrophysics for narrow resonances [20]. It is determined primarily by two exponential factors. The first one corresponds to the penetration factor through the Coulomb barrier strongly depending on the screening energy U_e . Its value increases by 20 orders of magnitude when changing U_e from 100 eV to 400 eV [9]. The second factor results from the enhanced deuteron diffusion at temperature kT in the local target region, where projectiles induce elastic collisions with target atoms and increase the number of moving thermal deuterons N . At beam energies lower than several keV, the nuclear stopping contribution responsible for the collision cascade grows with lowering deuteron energy oppositely to the electronic excitation of atoms (see Fig. 3a). The maximum of the nuclear stopping power for a ZrD₂ target is at 80 eV and is at a level similar to the electronic stopping. In the case of a pure metallic Zr target, the nuclear stopping power is lower and possesses a maximum at the deuteron energy 1.5 keV since the scattering on heavier atoms results in a lower energy loss. Although, the atomic collision cascades have a small lateral size of a few fm, and their range reaches a value of 21 nm at 2 keV [19], the bombarding deuterons produce a strong lattice oscillation related to a high number of phonons. The total deuteron beam energy transferred to the target by means of electronic excitation and atomic collisions are presented in Fig. 3b. The energy dissipation during the collision cascade can be described within the so-called elastic-collision spike model [21, 22, 23] that explains a strong increase of temperature within the ion tracks leading to crystal defects, local melting of the target material or even its change into a gaseous phase. This model was successfully extended to include also electronic excitations, which are important for interaction of swift heavy ions with matter [24, 25]. Here, only a simplified model will be used to determine the average temperature and size of the ion tracks.

Considering that the lateral size of the cascades does not strongly change with projectile energy, the total beam energy transferred to cascades, divided by the beam range should correspond to the phonon density excited in this region. As can be seen in Fig. 3b, the phonon density slightly decreases now for deuteron energies between 0.5 - 4 keV. However, following the thermal spike models of ion tracks we can assume that about 10% of the projectile energy stored into the electronic excitation [25,26] can be transferred to the lattice due to the electron-phonon coupling. Therefore, we finally can get an almost constant phonon density independent of the projectile energy (Fig. 3b). The phonon energy in the ϵ -ZrD₂ phase

amounts to about 100 meV and the related specific heat capacity is equal to 28 J/mol/K at room temperature [27]. According to the calculations performed with the TRIM code [19], the initial ion track volume amounts to $1 \text{ nm}^2 \times 21 \text{ nm} = 21 \text{ nm}^3$ for the 2 keV deuteron beam. The absorbed energy of 0.42 keV due to the collision cascades and 10% of the electronic excitation of 1.60 keV are transferred to the ion track and lead to the phonon density of about $580 \text{ eV}/0.1 \text{ eV}/21 \text{ nm}^3 = 280 \text{ phonons}/\text{nm}^3$. This results in the initial temperature within the ion track of about 2540°K , which is above the Zr melting temperature of 2127°K . This explains the ion track formation and the strong increase of the atomic diffusion in the hot regions. Therefore, the target surface undergoes significant changes (see Fig. 4) and results in a crystalline grain grow after low-energy ion irradiation [28]. The temperature within the ion tracks fast decreases, leading to its recrystallization and expending of high temperature region [24]. According to the Bose-Einstein statistics, room temperature can be reached after 10^{-10} seconds for a volume of 1870 nm^3 ($74 \text{ nm}^2 \times 24.8 \text{ nm}$) and a density $3.1 \text{ phonons}/\text{nm}^3$. The average temperature of the expanding ion track amounts to about 980°K . Similar calculation can be performed for a 1 keV deuteron beam. Since the deuteron range and the absorbed energy decrease to 11.4 nm and 364 eV , respectively, the initial phonon density slightly increases to the value of $319 \text{ phonons}/\text{nm}^3$ and the average track temperature reaches 1080°K .

To estimate the nuclear reaction rates, the number of moving deuterons in the crystal lattice is necessary. It can be calculated with the Arrhenius relation describing the deuteron diffusion in Zr:

$$N = N_0 \exp(-E_A/kT) \quad (5)$$

where E_A is the activation energy equal to $40.1 \pm 0.8 \text{ kJ/mol}$ (413 meV) [29]. The total number of moving deuterons within the ion track of a lifetime $\tau = 10^{-10} \text{ s}$ can be then calculated as a product $N/N_0 \cdot V$, where V stays for the track volume. The ratio N/N_0 at temperature of 1000°K is higher by 5 orders of magnitude than the value at room temperature. The track volumes for the deuteron energies 1 and 2 keV are almost equal and amounts to 13.0 nm^3 and 12.2 nm^3 , respectively. Thus, the phonon density within the ion track, deciding on the number of colliding deuterons and the thermal reaction rate, remains constant. The reduction of the track range for the decreasing beam energy is compensated by the increase of the initial track temperature.

The detected number of emitted thermal protons per second can be now achieved with the formula:

$$\mathcal{N}(T) = I \cdot V \cdot \tau \cdot \frac{\Omega}{4\pi} \cdot \mathcal{R}(T) \quad (6)$$

where the projectile current $I = 90 \mu\text{A}$ at deuteron energy 2 keV defines the number of tracks per second and Ω stays for the solid angle of the detector. For the average track temperature of 1080°K , track volume 1870 nm^3 , screening energy 340 eV and $\frac{\Omega}{4\pi} = 0.02$, we obtain one proton count per 10,000 s, which is about 3 times higher count rate than that observed in our experiment in the energy region of the yield plateau (see Fig. 2).

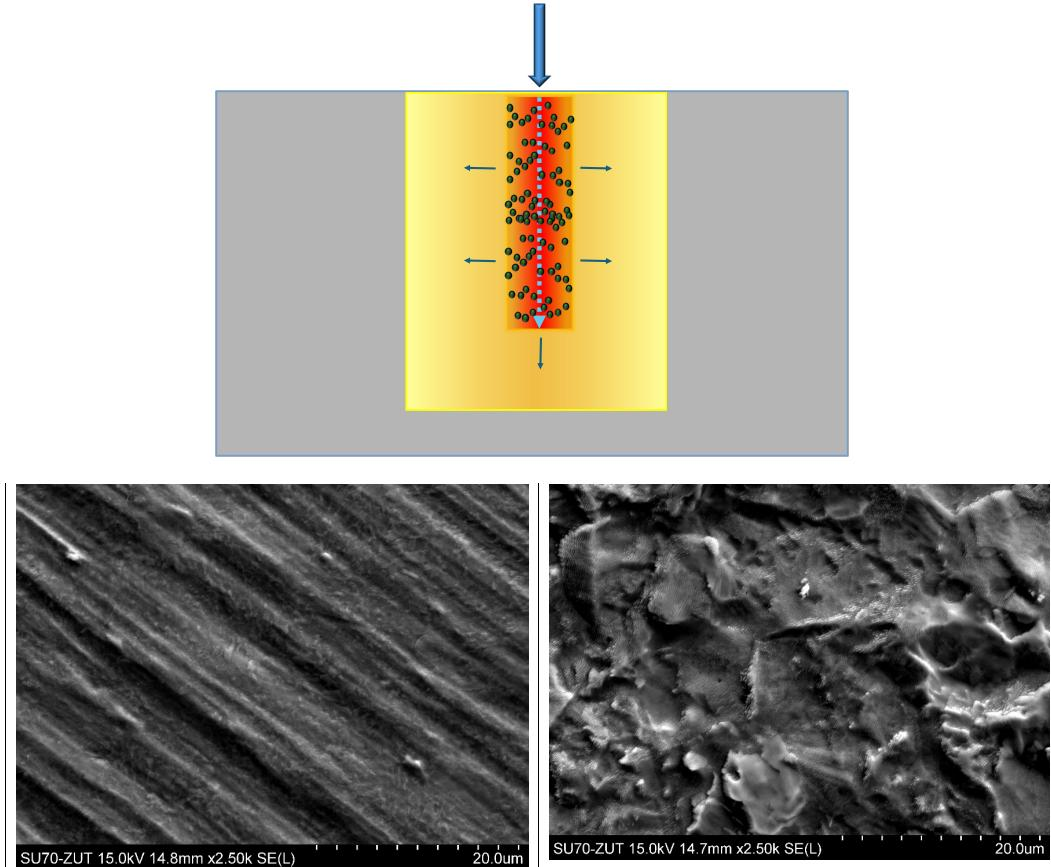


Fig. 4: Top: Illustration of an expanding ion track. Bottom: Scanning electron microscope (SEM) images of the Zr target before (left) and after long-term deuteron irradiation (right).

3. Discussion and conclusions

In view of the model simplification we have made, the agreement between the theoretical prediction and experiment is very convincing, confirming both the absolute numbers and the energy independence of yield for beam energies below 2.5 keV. The uncertainty in this estimate is relatively large and amounts to one to two orders of magnitude, mainly due to the uncertainty of the screening energy and electron-phonon coupling. However, these uncertainties should be considered in relation to the reaction rate which is about 20 orders of magnitude higher due to the electron screening effect and threshold resonance when compared to the value obtained for the defect free Zr target ($U_e = 100 \text{ eV}$). Similarly, the average ion track temperature of 1000°K leads to the increased deuteron diffusion in comparison to room temperature and results in the enhancement factor of the

fusion rate by 10 orders of magnitude (see Eq. 4 and 5). This last figure also shows how important the high temperature within ion tracks is for thermal proton emission. This could be also confirmed in our recent experiment [30] in which we have measured the DD fusion reaction occurring in Pd. The yield plateau effects have been observed at much higher deuteron energy of about $E_{LAB}=5$ keV, which is due to the much larger deuteron diffusion coefficient.

In summary, we have presented for the first time a thick-target yield measurement of the $^2\text{H}(\text{d},\text{p})^3\text{H}$ reaction down to the previously unavailable deuteron energy in CMS of 0.625 keV. The electron screening energy of 340 ± 30 eV estimated for the measurement over seven orders of magnitude agrees very well with results of previous experiments and could be recently explained by production of crystal lattice vacancies decorated by oxygen atoms [8,15]. At the lowest CMS deuteron energies below 1.25 keV, a thick-target yield plateau has been observed, which is about two orders of magnitude above the presumed contribution of neutralized deuterium ions. The protons emitted in this beam energy region have significantly higher energies than those expected for irradiation with neutralized deuterons and can be explained by the DD reactions occurring at thermal (meV) energies. According to calculations, the thermal DD reactions can take place in the ion tracks induced by the deuteron beam, where high phonon densities and temperatures above the melting point can be reached. Due to the locally increased deuteron diffusion, the model can explain both the absolute value of the effect and the observed reaction yield plateau at the lowest projectile energies. The achieved results confirm that DD reactions can take place at thermal energies due to high electron screening energies in the hosting metallic environments and the threshold resonance observed previously. An independent confirmation of high DD reaction rates at thermal energies can provide the last observation of a large number of emitted neutrons [31]. According to our model, the absolute yield of these effects can be modulated by the number of crystal lattice defects determining the electron screening energy, leading to an additional increase of reaction rates. This opens new perspectives for future materials research aimed at developing a new fusion energy source.

4. Methods

4.1 Experimental setup

The experiments were conducted at the eLBRUS Ultra High Vacuum Accelerator of the University of Szczecin, Poland. The facility combines a very good vacuum of 10^{-10} mbar in the target chamber with a high current ion beam up to 1 mA on the target [32]. Due to dropping cross sections of nuclear reactions at very low energies below the Coulomb barrier, an important feature of the accelerated ion beams is their very good energy definition of 10 eV and the long-term stability of about 5 eV, provided by the ECR ion source. The electric voltage put on the ion source with respect to the grounded target chamber gave directly the energy

of the accelerated charged particles. The beam energy precision and the selection of a Q/M beam components were ensured a 90° double focusing analyzing magnet equipped with a high precision Hall probe for B-field measurement. The accelerated system has been recently upgraded (see Fig. 6) and put on a special platform increasing or decreasing its potential compared to the target chamber at the ground potential. In front of the target chamber a decelerating system consisting of two electric lenses has been additionally installed. Thanks to the modification, the ion source could be operated at high potentials delivering high currents independent of the final beam energies. After deceleration, a beam current of several hundred microamps at the lowest projectile energies of about 1 keV, focused to a 7 mm diameter beam spot on the target could be achieved. The highest acceleration potential is 26 kV. The beam current stability measured on the target was better than 0.5%. Secondary electron emission from the target increased the ion beam charge collected only by 10-15% for the entire energy range of the used deuteron beam, which was checked by positively biasing the target holder with a voltage up to 60V.

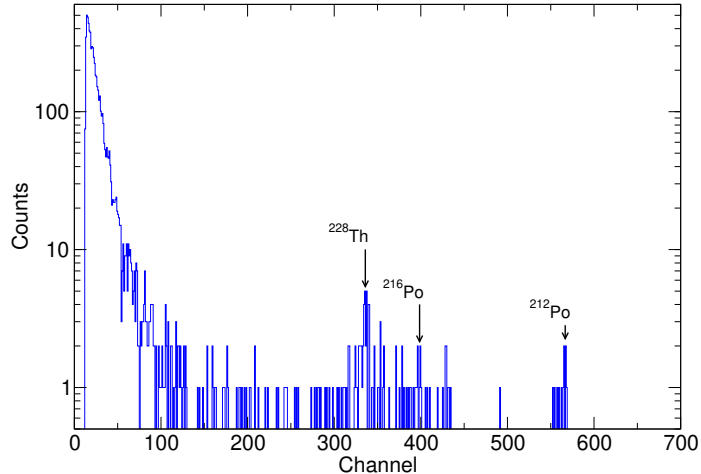


Fig. 5: Natural background spectrum characteristic for the ^{232}Th alpha-decay series: ^{228}Th 5.52 MeV, ^{216}Po 6.91 MeV, ^{212}Po 8.95 MeV. The energies measured are lower than the nominal decay values due to the energy loss of alpha particles in the protection foil in front of the Si detector. The spectrum was measured for 5 days.

In the present experiment, atomic and molecular deuteron beams D_1^+ , D_2^+ and D_3^+ , analyzed magnetically have been applied. The charged particles emitted in the DD reactions: 0.8 MeV ^3He , 1.02 MeV ^3H and 3 MeV protons have been registered by a low-noise PIPS Si detector (100 μm thick, 100 mm^2 detection area) placed at a distance 7 cm from the target, at an angle of 135° with respect to the beam. In front of the detector, a 1 μm thick aluminum foil has been located to prevent elastically scattered deuterons from entering the detector. The energy resolution of the detector was about 18 keV. As a target, a 1mm thick Zr plate implanted to the highest possible stoichiometry ZrD_2 has been applied. Deuterated Zr targets are known for their high stability and isotropic deuterium density distribution with small fluctuations of about 10%, as well as for their high electron screening energies [7]. The target

temperature was kept below 45°C by reducing the beam current at higher deuteron energies and using a special air-cooling system. The experimental setup has been presented in detail together with Monte Carlo simulations of particle spectra in [33].

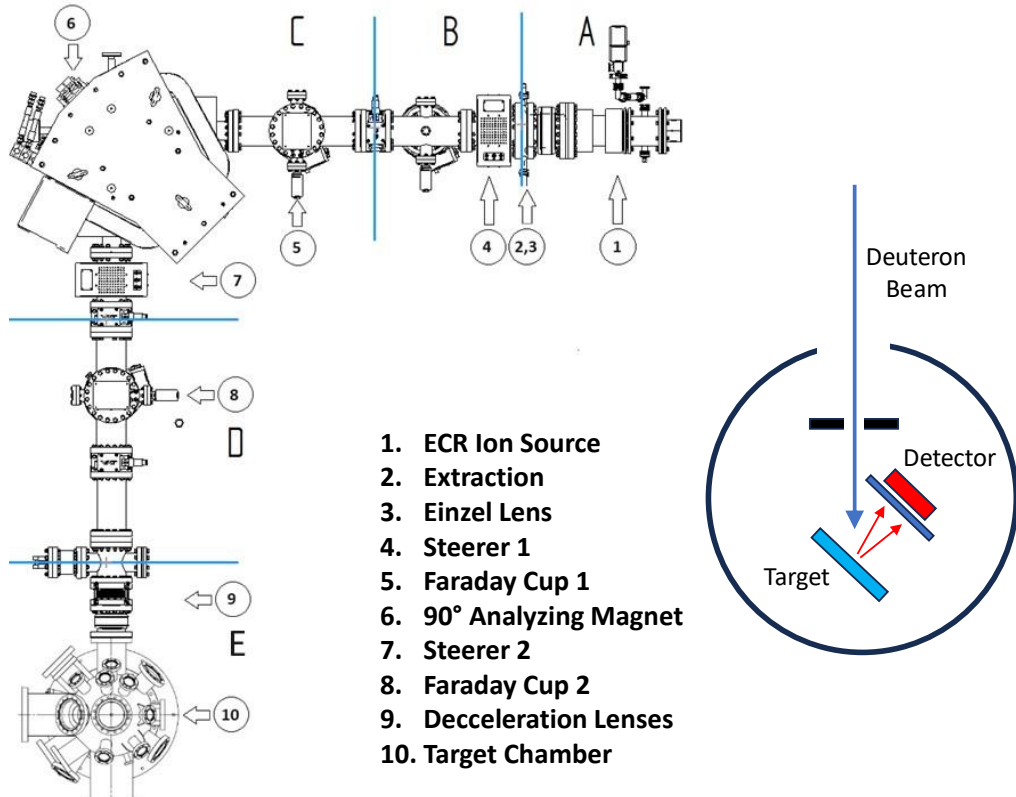


Fig. 6: Ultra-high vacuum accelerator system at the University of Szczecin, Poland. The displayed sections of the system correspond to different units of the differential pumping system. The right side shows the position of the detector in the target chamber relative to the deuteron beam.

Experimental spectra measured at different energies using atomic and molecular deuterium beams are displayed in Fig. 1. At the lowest beam energies, the spectra were collected for more than one week. A corresponding background in the energy region of the proton line of a few counts was subtracted. The stability of the energy calibration of the Si detector was repeatedly checked during the measurements by alternating short measurements at higher deuteron energies with measurements at lower energies, requiring longer measurement times. Additionally, at the lowest beam energies, energy calibration was also assured by controlling the line position of the natural background dominated by three main alpha-decays (see Fig. 5).

4.2 Thick target yield vs. reaction rate

The screened reaction cross-section below the Coulomb barrier can generally be expressed by the astrophysical S-factor:

$$\sigma_{scr}(E) = \frac{1}{\sqrt{E(E+U_e)}} S(E) \exp\left(-\sqrt{\frac{E_G}{E+U_e}}\right) \quad (7)$$

where the astrophysical S-factor $S(E)$ in absence of narrow resonances is usually a slowly changing function of the CM energy. In the low energy accelerator studies, the cross section cannot be determined directly as the range of projectiles is very low and the cross-section changes strongly. Instead, the thick target yield being a sum of the reaction contributions from different target depth is a standard quantity that can be obtained [35]:

$$Y_{scr}(E) = N_0 \int_0^R \sigma_{scr}(E) dx = N_0 \int_0^E \frac{\sigma_{scr}(E)}{|dE/dx|} dE \quad (8)$$

where the density of reacting nuclei in the target N_0 is assumed to be constant along of the pathway of projectiles up to their range R . The stopping power function $|dE/dx|$ has to components: electronic and nuclear. The electronic part describes energy loss mechanisms related to atomic excitation and ionization which is proportional to \sqrt{E} in the low energy limit. For projectile energies below 1 keV, the nuclear stopping power associated with scattering on lattice atoms begins to dominate. Since the yield function decreases exponentially with lowering energies and our experiments are performed for deuteron energies higher than 1 keV, we can approximate the stopping power value as $|dE/dx| = C\sqrt{E}$, which leads to an expression:

$$Y_{scr}(E) = N_0 \int_0^E \frac{\sigma_{scr}(E)}{C\sqrt{E}} dE = \frac{N_0}{C} \int_0^E \frac{\frac{1}{\sqrt{E(E+U_e)}} S(E) \exp\left(-\sqrt{\frac{E_G}{E+U_e}}\right)}{\sqrt{E}} dE \quad (9)$$

This integral can be calculated analytically:

$$Y_{scr}(E) = \frac{2N_0 S(E)}{C\sqrt{E_G}} \left[\exp\left(-\sqrt{\frac{E_G}{E+U_e}}\right) - \exp\left(-\sqrt{\frac{E_G}{U_e}}\right) \right] \simeq \frac{2N S(E)}{C\sqrt{E_G}} \exp\left(-\sqrt{\frac{E_G}{E+U_e}}\right) \quad (10)$$

assuming that the astrophysical S-factor does not change strongly and that $E \gg U_e$. The S-factor is a coherent sum of a broad resonance contribution S_B and the narrow 0^+ threshold resonance [7,9] S_R :

$$S(E) = S_B + S_R(E) + 2 \left(\frac{1}{3} S_B S_R(E) \right)^{1/2} \cos(\varphi_B^{0+}) \quad (11)$$

where $S_B = 57$ keV b is taken as a constant [14], and only one third of its value contributes to the interference effect. The resonance component can be described by a Breit-Wigner formula:

$$\sigma_R(E) = \frac{\pi}{k^2} \frac{\Gamma_d \Gamma_p}{(E - E_R)^2 + \Gamma^2/4} \simeq \frac{\pi}{k^2} \frac{\Gamma_d \Gamma_p}{E^2} \quad (12)$$

Here we consider $E_R \rightarrow 0$. The deuteron partial width Γ_d takes the value for the single-particle resonance:

$$\Gamma_d(E + U_e) = 2kaP(E + U_e) \frac{\hbar^2}{\mu a^2} = 2k \frac{\hbar^2}{\mu a} (E_G/(E + U_e))^{1/2} \exp[-(E_G/(E + U_e))^{1/2}] \quad (13)$$

and

$$S_R(E) = \frac{(2E_G)^{1/2} \hbar^3}{a \mu^{3/2}} \frac{\Gamma_p}{E^2} \quad (14)$$

where Γ_p is the proton partial resonance width, and a and μ stay for the DD channel radius of 7 fm and the reduced mass, respectively. Since the resonance contribution to the thick target yield in the energy range studied is relatively low compared to a strong screening enhancement, the screening curves presented in Fig. 2 and 3 do not include resonance contribution and the S-factor was assumed to be constant.

Oppositely to the standard accelerator experiments, where a projectile reacts with resting target nuclei, in the case of the classical plasma at temperature kT , where all the constituents interact with each other, the nuclear reaction rate is a proper quantity to describe the observed number of reactions:

$$\mathcal{R}(T) = \frac{N^2}{2} \langle \sigma v \rangle = \frac{N^2}{2} \frac{(8/\pi)^{1/2}}{\mu^{1/2} (kT)^{3/2}} \int_0^\infty \sigma(E) E \exp(-E/kT) dE \quad (15)$$

Here we assumed the classical Maxwell-Boltzmann velocity distribution. In the case of a narrow Breit-Wigner resonance, considering that its resonance strength is distributed over a small thermal energy spectrum, we get:

$$\mathcal{R}(T) = \frac{N^2}{2} \left(\frac{2\pi}{\mu kT} \right)^{3/2} \hbar^2 \exp(-E_R/kT) \frac{\Gamma_d \Gamma_p}{\Gamma} \quad (16)$$

The expression for the deuteron single-particle resonance width (Eq.13) at $E = 0$ finally leads to:

$$\mathcal{R}(T) = N^2 \frac{16\pi^{3/2} \hbar^3 E^{1/2}}{\mu^2 a (kT)^{3/2}} (E_G/U_e)^{1/2} \exp[-(E_G/U_e)^{1/2}] \exp(-E_R/kT) \frac{\Gamma_p}{\Gamma} \quad (17)$$

The screening function $\exp[-(E_G/U_e)^{1/2}]$ is the main factor deciding on the absolute value of the reaction rate. However, the number density N strongly depends on the temperature,

as well. Its value can be correlated to the diffusion coefficient and can be expressed as $N = N_0 \exp(-E_A/kT)$, where E_A denotes the activation energy, equal to 413 meV for ZrD₂ [29]. The local temperature within the ion track induced by bombarding deuterons is related to a number of excited phonons described by the well-known nuclear stopping power function [19].

4.3 Experimental thick target yield and proton peak position

The experimental thick target yield in the deuteron energy range of the observed yield plateau can be described as a sum of two components: the strongly energy dependent direct part and the constant contribution resulting from the thermal fusion. The corresponding formula can be presented as follows:

$$Y_{tot}(E) = Y_{scr}(E) + \mathcal{R}(T)_{exp} \quad (18)$$

Here, $Y_{scr}(E)$ describes the experimental dependence of the thick target yield determined at higher deuteron energies (see Eq. 10):

$$Y_{scr}(E) = M \exp\left(-\sqrt{\frac{E_G}{E+U_e}}\right) \quad (19)$$

which is fitted to the experimental data using the normalization factor M and the screening energy U_e as it is presented in Fig.2a and Fig. 7a. The thermal fusion contribution $\mathcal{R}(T)_{exp}$ can be then compared with theoretical calculations based on Eq. 17.

The peak position of 3 MeV protons could be determined with an uncertainty of 0.2 channel corresponding to about 3 keV by fitting a Gaussian function for measurements performed at higher deuteron energies, resulting in relatively high count statistics. For lower energies, with fewer than 40 proton events, the mean value of the count distribution and its variance were calculated using the standard formulas:

$$\langle x \rangle = \sum_i n_i x_i / \sum_i n_i \quad \text{and} \quad \langle x^2 \rangle = \sum_i n_i (x_i - \langle x \rangle)^2 / \sum_i n_i \quad (20)$$

where x_i and n_i are the channel number and the corresponding number of counts, respectively. The method is independent of the actual distribution function, which is an advantage since the line shape is not fully Gaussian. In this case, we set one-third of the variance as the uncertainty of the peak position being of about 0.5 channel, corresponding to 7.5 keV (see Fig. 2b and 7b).

The experimentally determined proton peak position $x_p(E)$ could be then described by a weighted average of two values arising from reaction kinematics and a constant energy value of protons emitted from a resting CM system (thermal fusion):

$$x_p(E) = \frac{Y_{scr}(E) \cdot x_{kin}(E) + \mathcal{R}(T)_{exp} \cdot x_{kin}(0)}{Y_{scr}(E) + \mathcal{R}(T)_{exp}} \quad (21)$$

where $x_{kin}(E)$ can be obtained from the reaction kinematics:

$$x_{kin}(E) = a \cdot \left(\frac{3}{4}Q + \frac{1}{2}E(1 + \cos^2\varphi) + \sqrt{E} \cos\varphi \sqrt{\frac{3}{4}Q + \frac{1}{4}E(2 + \cos^2\varphi)} \right) + b \quad (22)$$

Here, Q is the Q-value of the ${}^2\text{H}(\text{d},\text{p}){}^3\text{H}$ reaction, and φ is the detection angle with respect to the beam. The parameters a and b represent the linear energy calibration of the detector as slope and offset, respectively. The offset takes into account the proton energy loss in the aluminum protection foil placed in front of the Si-detector of about 22 keV corresponding to 1.5 channel. The detection angle φ could be independently fitted to experimentally determined proton peak positions (see the black “kinematic” curve in Fig. 2b and 7b). The obtained value of $138^\circ \pm 4^\circ$ agrees very well with the actual angle.

4.4 Beam neutralization effect

Despite very good vacuum in the target chamber, the differential pumping system gradually reduces the vacuum pressure at the ion source of 10^{-6} mbar to the value of 5×10^{-9} mbar in the beam line behind the analyzing magnet. Due to increasing cross sections of charge exchange reactions on hydrogen molecules for lowering energies, a fraction of the ion beam can be neutralized in this part of the beam line and is not decelerated by the electric lenses in front of the target chamber. Considering 1.5 m distance between the electric beam steerer and the deceleration lenses and the neutralization cross section [17,18,34] of 10^{-15} cm 2 at 8×10^{-9} mbar rest gas pressure, the fraction of neutral beam can be estimated to about 6×10^{-5} . This value is very close to the experimentally determined fractions for the D_2^+ beam of approximately 10^{-4} (see Fig. 2a), which is especially important for measurements of strongly decreasing reaction cross sections.

Experimentally, we can observe the neutralization effect as a slightly increasing plateau in the reaction yield measured at extremely low energies since the neutralization cross section increases for lowering energies. The main argument for the neutralization origin of the observed D_2^+ yield plateau is the energy of emitted protons. The proton peak position is lower than would result from the decelerated beam energy; instead, it corresponds to the peak position of the high energy deuterons (Fig. 2b).

Similar effects can also be observed for the atomic D_1^+ beam (see Fig. 7). A slightly increasing plateau can be observed towards lower deuteron energies with reaction yield values about two orders of magnitude higher (and higher beam energies) than in the case of the molecular D_2^+ beam, while the neutralization factor remains at the same level of about 3×10^{-4} . In Fig. 7a, the “screened” yield functions corresponding to $U_e=340\text{ eV}$ (Eq. 19) and the curve without screening ($U_e=0$) are displayed, as well. The red full curve is a sum of $Y_{scr}(E)$ and the reaction yield resulting from the beam neutralization. The latter is assumed to be linearly decreasing with energy and was fitted to the data obtained for energies below 6 keV. The dashed blue horizontal lines in Fig. 7a serve to compare reaction yields at 20 keV and 6 keV and determine the neutralization factor. Slightly increasing plateau yield towards lowering projectile energies is in agreement with experimental data and theoretical calculations of the collisional recombination of D_1^+ and D_2^+ ions on deuterium D_2 molecules [18].

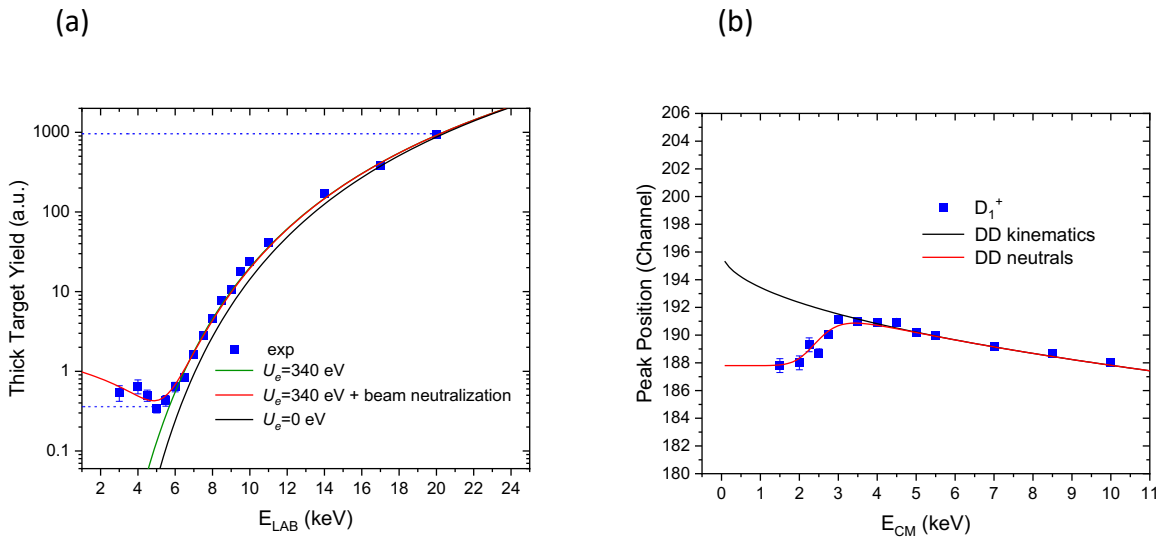


Fig. 7: (a) Thick target yield of the $^2\text{H}(\text{d},\text{p})^3\text{H}$ reaction measured using the atomic D_1^+ beam. The green full line corresponds to a theoretical curve obtained for the screening energy $U_e=340 \pm 30\text{ eV}$ according to Eq. 19. The black full line represents the theoretical curve for $U_e=0$. The red curve results from slightly increasing neutralization cross section for lowering projectile energies and the green screening curve. The blue dashed lines show yield values obtained for the about 3×10^{-4} fraction of the neutralized D_1^+ beam (plateau) compared to the yield measured at 20 keV. (b) Channel number of the proton peak position. At the lowest deuteron energies, the experimental data obtained with the D_1^+ beam can be described by the neutral yield component corresponding to 20 keV deuterons. The related points are much lower than the theoretical values calculated according to the reaction kinematics (black curve). The red curve takes into account both the reaction kinematics and the neutralization effect.

The beam neutralization process is supported by the observed proton peak position (see Fig. 7b). The proton energies measured for the beam decelerated below 6 keV are systematically lower than that expected from the reaction kinematics and reach the lowest value corresponding to that observed for 20 keV (CMS energy of 10 keV). The red curve in Fig. 7b is calculated as a weighted sum of two components: the “screened” yield function and

the neutralization yield, similarly to the procedure applied to the thermal fusion yield (see Eq. 21).

Data availability

The datasets presented in Fig.2 and Fig.7 of this manuscript are available at: <https://doi.org/10.18150/33ZBS0>. All other experimental data are available from the corresponding authors upon request.

Acknowledgements

The study is part of the CleanHME project from the European Union's Horizon 2020 research and innovation program under grant agreement No 951974.

References

1. Spitaleri C, Bertulani C A, Fortunato L, Vitturi A 2016 The electron screening puzzle and nuclear clustering, *Phys. Lett. B* **755** 275-278
2. Czerski K, Huke A, Heide P, Ruprecht G 2001 Enhancement of the electron screening effect for d + d fusion reactions in metallic environments, *Europhys. Lett.* **54** 449-455
3. Kasagi J, Yuki H, Baba T, Noda T, Taguchi J, Shimokawa M, Galster W 2004 Strongly Enhanced Li + D Reaction in Pd Observed in Deuteron Bombardment on PdLi_x with Energies between 30 and 75 keV, *J. Phys. Soc. Jpn.* **73** 608-612
4. Cruz J et al. 2005 Electron screening in ⁷Li(p,α)α and ⁶Li(p,α)³He for different environments, *Phys. Lett. B* **624**, 181-185.
5. Cvetinovic A et al. 2015 Molecular screening in nuclear reactions, *Phys. Rev. C* **92** 065801
6. Ichimaru S 1999 Pycnonuclear reactions in dense astrophysical and fusion plasmas, *Physics of Plasmas* **6** 2649-2671
7. Czerski K et al. 2016 Screening and resonance enhancements of the 2H(d, p)3H reaction yield in metallic environments, *EPL* **113** 22001
8. Kowalska A et al. 2025 Electron Screening in Deuteron–Deuteron Reactions on a Zr Target, *Materials* **18** 1331
9. Czerski K 2022 Deuteron-deuteron nuclear reactions at extremely low energies, *Phys. Rev. C* **106** L011601
10. Czerski K et al. 2024 Indications of electron emission from the deuteron-deuteron threshold resonance, *Phys. Rev. C* **109** L021601
11. Haridas Das G et al. 2024 High-energy electron measurements with thin Si detectors, *Measurement* **228** 114392
12. Dubey R et al. 2025 Experimental signatures of a new channel of the DD reaction at very-low energy, *Phys. Rev. X* **15** 041004
13. Kasagi J et al. 2002 Strongly Enhanced DD Fusion Reaction in Metals Observed for keV D+ Bombardment, *J. Phys. Soc. Jpn.* **71**, 2881-2885
14. Huke A et al. 2008 Enhancement of deuteron-fusion reactions in metals and experimental implications, *Phys. Rev. C* **78**, 015803

15. Kowalska A et al. 2023 Crystal Lattice Defects in Deuterated Zr in Presence of O and C Impurities Studied by PAS and XRD for Electron Screening Effect, *Materials* **16** 6255
16. Arai K et al. 2011 Tensor Force Manifestations in Ab Initio Study of the $^2\text{H}(\text{d},\gamma)^4\text{He}$, $^2\text{H}(\text{d},\text{p})^3\text{H}$, and $^2\text{H}(\text{d},\text{n})^3\text{He}$ Reactions, *Phys. Rev. Lett.* **107** 132502
17. Phelps A V 1990 Cross Sections and Swarm Coefficients for H^+ , H_2^+ , H_3^+ , H , H_2 , and H^- in H_2 for Energies from 0.1 eV to 10 keV, *Journal of Physical and Chemical Reference Data* **19**, 653-675
18. McClure G W 1963 Charge Exchange and Dissociation of H^+ , H_2^+ and H_3^+ Ions Incident on H_2 Gas, *Phys. Rev.* **130**, 1852-1859
19. Ziegler J F, Biersack J P and Littmark U 1985 *The Stopping and Range of Ions in Solids*, vol. 1 of *The Stopping and Ranges of Ions in Matter*, Pergamon Press, New York
20. Illiadiis C 2015 Nuclear Physics of Stars *Wiley-VCH Verlag GmbH*
21. Sigmund P 1974 Energy density and time constant of heavy-ion-induced elastic-collision spikes in solids, *Appl. Phys. Lett.* **25** 169-171
22. Sigmund P, Claussen C 1981 Sputtering from elastic-collision spikes in heavy-ion-bombarded metals, *J. Appl. Phys.* **52** 990-993
23. Schenkel T, Barnes A V, Hamza A V, Schneider D H, Banks J C and Doyle B L 1998 Synergy of Electronic Excitations and Elastic Collision Spikes in Sputtering of Heavy Metal Oxides, *Phys. Rev. Lett.* **80** 4325-4328
24. Dufour C and Toulemonde M 2016 Models for the Description of Track Formation, in W. Wesch and E. Wendler (eds.), *Ion Beam Modification of Solids*, Springer Series in Surface Sciences 61, p. 63-104
25. Giri A et al. 2020 Electron-phonon coupling and related transport properties of metals and intermetallic alloys from first principles, *Materials Today Physics* **12**, 100175
26. Zhang, Y. & Weber, W. J. Ion irradiation and modification: The role of coupled electronic and nuclear energy dissipation and subsequent nonequilibrium processes in materials, *Appl. Phys. Rev.* **7**, 041307 (2020).
27. Olsson P A T et al. 2014 Ab initio thermodynamics of zirconium hydrides and deuterides, *Computational Materials Science* **86** 211-222
28. Kaoumi D, Motta A T and Birtcher R C 2008 A thermal spike model of grain growth under irradiation, *J. App. Phys.* **104** 073525
29. Long X et al. 2011 Hydrogen Isotope Effects of Ti, Zr Metals, *Fusion Science and Technology* **60**, 1568-1571
30. Czerski K et al., to be published.
31. Kuo-Yi Chen et al. 2025 Electrochemical loading enhances deuterium fusion rates in a metal target, *Nature* **644** 640-645
32. Kaczmarski M et al. 2014 New accelerator facility for measurements of nuclear reactions at energies below 1 keV, *Acta Phys. Pol. B* **45** 509-518
33. Haridas Das, G. et al. High-energy electron measurements with thin Si detectors, *Measurement* **228**, 114392 (2024).
34. Tabata T and Shiray T 2000 Analytic Cross Sections for Collisions of H^+ , H^+ , H^+ , H , H_2 , and H^- with Hydrogen Molecules, *Atomic Data and Nuclear Data Tables* **76** 1–25
35. Czerski K et al. 2004 The $^2\text{H}(\text{d},\text{p})^3\text{H}$ reaction in metallic media at very low energies, *Europhys. Lett.* **68** 363-369